Biochimica et Biophysica Acta 1818 (2012) 829–838

Contents lists available at SciVerse ScienceDirect

Biochimica et Biophysica Acta

journal homepage: www.elsevier.com/locate/bbamem

Strain, stress and energy in lipid bilayer induced by electrostatic/electrokinetic forces

M. Tajparast [a], M.I. Glavinović [b,*]

[a] Department of Civil Engineering and Applied Mechanics, McGill University, Montreal, PQ, Canada
[b] Department of Physiology, McGill University, Montreal, PQ, Canada

ARTICLE INFO

Article history:
Received 23 May 2011
Received in revised form 14 September 2011
Accepted 18 October 2011
Available online 25 October 2011

Keywords:
Lipid bilayer
Normal stress
Shear stress
Dielectric force
Maxwell stress
Poisson–Nernst–Planck

ABSTRACT

Lipid bilayer was deformed by the electrostatic/electrokinetic forces induced by the fixed charges on the top monolayer–solution interface. The strains, stresses and energy were simulated using finite element method. The elastic moduli of the heads were four times greater than those of tails sections, but were individually isotropic. The physics of the situation was evaluated using a coupled system of linear elastic equations and electrostatic–electrokinetic (Poisson–Nernst–Planck) equations. The Coulomb force (due to fixed charges in the electric field), and the dielectric force (due to uneven electric field and the solution-membrane permittivity mismatch) bend the membrane, but unevenly. Whereas the bottom monolayer extends vertically (towards charged surface), the top monolayer compresses. In contrast the top monolayer extends horizontally, but the bottom monolayer compresses. The horizontal normal stress is higher in the heads than in the tails sections, but is similar in two monolayers, whereas the vertical normal stress is small. The horizontal normal stress is associated with horizontal normal strain, and vertical with both vertical and horizontal strain. Surprisingly, the shear stress (an indicator where the membrane will deform), is greater in the tails sections. Finally, the elastic energy (which is clearly greater in the heads sections) is dominated by its horizontal component and peaks in the middle of the membrane. The shear component dominates in the tails sections, and is minimal in the membrane center. Even spatially uniform external force thus leads to complex membrane deformation and generates complex profiles of stress and elastic energy.

© 2011 Elsevier B.V. All rights reserved.

1. Introduction

The membrane plays numerous roles and influences or critically determines the functioning of the cells or cellular organelles. The membrane delineates the boundaries of cells and compartmentalizes cellular organelles, and modulates the functioning of a variety of biological processes, and this often depends on the membrane shape. The shape, which is often intricate, thus has to be regulated precisely [1,2]. As argued persuasively in several studies the membrane curvature is to a significant extent determined by the elastic interactions between embedded proteins and the membrane [3,4,2]. Such interactions may in turn influence the spatial distribution of membrane proteins [5] and their function [6]. Finally, if the individual membrane proteins undergo conformational changes, this can also be communicated via deformations they cause in the elastic bilayer to the surrounding membrane proteins, and may further influence how the membrane proteins are spatially organized, and how they function. Individually, bilayer thickness, spontaneous curvature and bending stiffness can each modulate the function of membrane proteins [7,8].

For example the gating properties of mechano-sensitive (MS) channels, whose role is to respond to membrane mechanical stress, and which are influenced by the mechanical conditions of the membrane, depend on membrane curvature [9]. In prokaryotic cells [10,11,12] and in some eukaryotic MS channels [13], the transduction mechanism of MS channels responds directly to bilayer deformations and occurs at the protein–lipid interface. In contrast MS channels of other eukaryotic cells respond to mechanical deformations through the cytoskeletal network [14]. The membrane stresses probably influence not only the functions of MS channels, but also other channels and other proteins and lipids embedded in the biological membrane by modifying the "working" condition for their activity [15,16]. The membrane stress can alter the dimerization kinetics of the channel-forming peptide gramicidin A [17]. Hyposmotic swelling in pituitary cells directly modulates calcium influx through L-type channels, which plays a critical role in regulating basal and evoked transmitter or hormone secretion in a variety of secretory cells [18,19], and alters the hormone secretion [20]. Given that swelling leads to a higher membrane tension, the calcium channels probably directly sense change in membrane tension [21,22], which influences their gating. The mechanical state of the membrane can also have a large effect on the function of a voltage dependent K channel [23]. Finally, the membrane tension may also directly modulate exocytosis and endocytosis, with greater membrane tension stimulating the exocytosis, but suppressing the endocytosis [24].

* Corresponding author at: Department of Physiology, McGill University, 3655 Sir William Osler Promenade, Montreal, PQ, Canada H3G 1Y6. Tel.: +1 514 398 6002; fax: +1 514 398 7452.
E-mail address: mladen.glavinovic@mcgill.ca (M.I. Glavinović).

0005-2736/$ – see front matter © 2011 Elsevier B.V. All rights reserved.
doi:10.1016/j.bbamem.2011.10.018

Given that membrane stresses may be influencing the function and spatial distribution of a variety of membrane proteins and the fact that the reshaping of the membrane bilayer occurs on a wide length scale (ranging from the micrometer to nanometer), better understanding of the stresses and their spatial distribution is needed. We evaluated the strains, stresses and elastic energy within the membrane bilayer bent by a spatially uniform and constant electrostatic force induced by an asymmetrically charged membrane placed in a liquid electrolyte [25]. The electrostatic/electrokinetic forces were estimated by evaluating a coupled system of electrostatic/electrokinetic (Poisson–Nernst–Planck) equations [26,27,28], and strains, stresses and elastic energy within the membrane were evaluated using linear elastic equations [29,30,31]. The ionic concentrations and composition were as encountered physiologically [25].

Although the basic aspects of membrane bending can be studied by considering the membrane as an elastic surface [1,32], the focus of this study is in determining what the strains and stresses are within the membrane. We thus took into account its finite thickness and different elastic properties of heads and tails sections [2]. The elastic moduli of the heads and tails sections were different, but were individually both homogeneous and isotropic [25]. The simulations demonstrate that the stresses are distributed very unevenly in the bilayer. Briefly, the horizontal normal stress dominates in the heads sections, the shear stress in the tails sections, and the vertical normal stress is small everywhere.

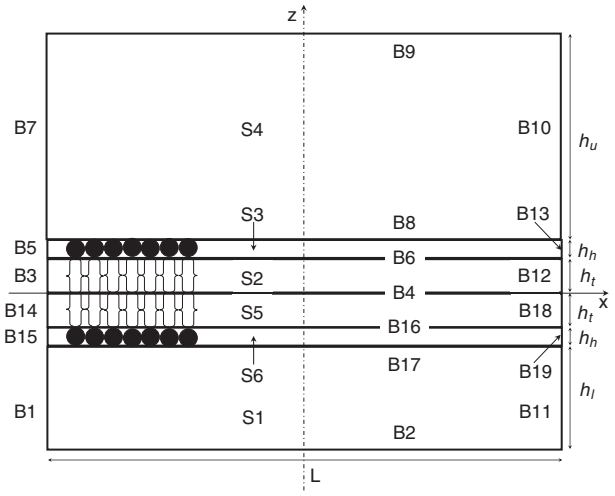

Fig. 1. Schematic representation of the lipid bilayer in the x–z plane. The membrane height h is divided into the hydrophilic heads (closed circles) with the height h_h and the hydrophobic tails (h_t) sections. L is the membrane length, and h_u and h_l are the heights of the upper and lower compartments with the electrolyte solution. The membrane plane is centered at the origin, and its thickness t_m is 100 nm. L is 20 nm, h is 2 nm, $h_h = 0.7$ nm, $h_u = 8$ nm, and $h_l = 4$ nm. S_i (i = 1–6) and B_j (j = 1–19) stand for the subdomains and boundaries of the lipid bilayer, respectively, and are defined in Table 1.

2. Methods

We evaluated numerically the deformation of a segment of the membrane lipid bilayer due to the presence of fixed charges on the internal side of the bilayer, but also due to the potential difference between two compartments bathing the membrane containing an electrolyte solution made of K^+, Cl^- (intracellular or upper compartment) or Na^+ and Cl^- (extracellular or lower compartment). The flat lipid membrane is considered as a two-dimensional (2-D) sheet in the x–y plane of the Cartesian coordinate system (x, y, z) with the center of the lipid bilayer in the origin. Fig. 1 depicts the schematic representations of the lipid bilayer. To account for the amphiphilic, and in turn anisotropic, nature of each lipid monolayer, we divide it into two sections — a hydrophilic heads section and a hydrophobic tails section. The height of the lipid monolayer h is 2 nm, its heads section h_h is 0.7 nm, whereas the tails section h_t is 1.3 nm (or as otherwise specified). The length of the membrane $L = 20$ nm (or in some simulations 40 nm or 80 nm), and its thickness t_m is 100 nm. h_u (= 8 nm) and h_l (= 4 nm) denote the heights of the upper and lower compartment, respectively. The subdomains and boundaries of the lipid bilayer are S_i and B_j respectively, where i = 1–6 and j = 1–19.

To analyze the structural deformation of the lipid membrane we consider the plane-stress model in the associated subdomains (i.e., 2, 3, 5, and 6). In contrast, the Poisson equation describing the electrostatics is defined in all the subdomains. The Nernst–Planck equation describes the electrokinetic flow and accounts for the movement (i.e., diffusion and migration) of ions in the electrolyte media and is active in subdomains 1 and 4. The membrane is assumed to be impermeable to movement of ions. Table 1 gives all boundary conditions and Table 2 details the model parameters and constants. In the companion paper we described in detail how to calculate all electrostatic (potential, electric field, space charge density), electrokinetic variables (concentrations), but also electrostatic forces (Coulomb and dielectric) and stresses (Maxwell stress). In the Appendix of the same paper we gave all equations for the structural analysis and showed how to evaluate the elastic strains, stresses, surface traction and elastic energy for an isotropic and an anisotropic membrane bilayer [25]. Finally, the numerical evaluation of the system of coupled equations given by the Poisson–Nernst–Planck and elastic equations was done using finite element method and a commercial software package program Comsol 3.5 (Comsol, Burlington, MA, USA), whereas the postprocessing was performed using a software package for scientific and engineering computing Matlab (MathWorks, Natick, MA, USA).

3. Results

3.1. Membrane deformation

How does the membrane deform as it is pulled up by the electrostatic (Coulomb and dielectric) forces? Fig. 2A gives the horizontal plot of the vertical displacement of the top and bottom membrane surface, and it is clear that even when the vertical displacement is significant, the difference in displacement is small. Nevertheless, it is of interest to

Table 1
Boundary conditions.

Boundary	Plane Stress	Electrostatics	Electro-kinetics
B1, B7, B10, B11	NA	Zero charge symmetry	Insulation symmetry
B2	NA	Electric potential V_d	Concentration C_{i0d}
B3, B5, B12, B13, B14, B15, B18, B19	x–y symmetry plane	Zero charge symmetry	NA
B4, B6, B16	Continuity	Continuity	NA
B8	Prescribed displacement: u and w in x and z directions, respectively; applied total force due to Maxwell stress tensor and charged surface (F_{e8})	Surface charge density σ_{e8}	Insulation symmetry
B9	NA	Electric potential V_u	Concentration C_{i0u}
B17	Prescribed displacement: u and w in x and z directions, respectively; Applied force due to Maxwell stress tensor (F_{e17})	Surface charge density σ_{e17}	Insulation symmetry

Table 2
Model parameters and constants.

Params	Value	Description	Unit	Refs
C_{10u}	150.0	K^+ concentration (upper compartment)	mol/m^3 or mM	
C_{20u}	150.0	Cl^- concentration (upper compartment)	mol/m^3 or mM	
C_{30u}	0	Na^+ concentration (upper compartment)	mol/m^3 or mM	
C_{10d}	0	K^+ concentration (lower compartment)	mol/m^3 or mM	
C_{20d}	150.0	Cl^- concentration (lower compartment)	mol/m^3 or mM	
C_{30d}	150.0	Na^+ concentration (lower compartment)	mol/m^3 or mM	
D_1	1.960×10^{-9}	Diffusion coefficient of K^+ ions	m^2/s	[28,35]
D_2	2.030×10^{-9}	Diffusion coefficient of Cl^- ions	m^2/s	[28,35]
D_3	1.330×10^{-9}	Diffusion coefficient of Na^+ ions	m^2/s	[28,35]
e	1.602×10^{-19}	Elementary charge	C	
R	8.314	Universal gas constant	J/(mol.K)	
T	300.0	Temperature	K	
V_u	-8.000×10^{-2}	Electric potential (controlling edge of the upper compartment)	V	
V_d	0	Electric potential (controlling edge of the lower compartment)	V	
e_0	8.854×10^{-12}	Permittivity of vacuum	F/m	
e_{rw}	80.0	Relative permittivity of the electrolyte media	Dimensionless	[27,26]
e_{rm}	2.0	Relative permittivity of the membrane	Dimensionless	[28]
ρ_m	785.0	Membrane density	kg/m^3	[28]
σ_{e8}	-8.000×10^{-3} or as specified	Surface charge density of the upper boundary of the membrane bilayer (B8)	C/m^2	[34,35]
σ_{e17}	0	Surface charge density of the lower boundary of the membrane bilayer (B17)	C/m^2	
ν	0.330	Poisson's ratio	Dimensionless	
λ_{mhxxxx}	4.000×10^9	Young's modulus of volume stretching-compression in lateral direction (heads)	Pa	[2]
λ_{mhxxzz}	3.930×10^9	Young's modulus of coupling between lateral and normal deformation (heads)	Pa	[2]
λ_{mhzzzz}	4.000×10^9	Young's modulus of volume stretching-compression in normal direction (heads)	Pa	[2]
λ_{mtxxxx}	1.000×10^9	Young's modulus of volume stretching-compression in lateral direction (tails)	Pa	[2]
λ_{mtxxzz}	0.980×10^9	Young's modulus of coupling between lateral and normal deformation (tails)	Pa	[2]
λ_{mtzzzz}	1.000×10^9	Young's modulus of volume stretching-compression in normal direction (tails)	Pa	[2]

find to what extent the membrane extends (or compresses) vertically, and whether the change is uniform. Fig. 2B depicts the cross-sectional plot of the vertical displacement in the membrane center ($x=0$ nm) and 5 nm to the right of the membrane center for a 20 nm membrane segment, but also for longer 40 nm segment. In order to evaluate whether all elements of the membrane are equally displaced, but also to compare the displacement at two loci we normalized their vertical displacement at the bottom of the membrane (i.e. we set them to zero). The membrane is displaced progressively more and more starting from the bottom of the membrane towards the top (i.e. the membrane is vertically extended), although the difference is very small compared to the thickness of the membrane. At the peak of the displacement the difference amounts to just above 0.004 nm in the membrane center,

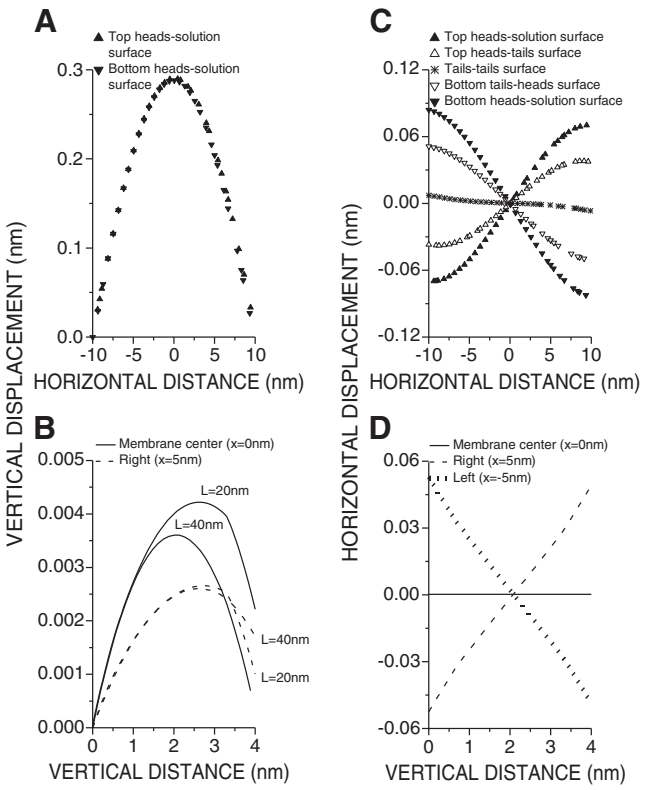

Fig. 2. The membrane extends horizontally and compresses vertically in the top monolayer, whereas opposite is true in the bottom monolayer. A) Horizontal profile of the vertical displacement of the top heads-solution surface and the bottom heads-solution surface. B) Vertical profile of the vertical displacement of the membrane in the membrane center ($x=0$ nm), and at 5 nm to the right for a 20 nm segment (as in all other panels) and for a 40 nm segment (as indicated). For better comparison, the vertical displacement is set to zero at the bottom of the membrane. Note that the membrane is vertically extended (bottom monolayer), but is compressed (top monolayer) as it is pulled up by the action of the electrostatic forces, especially in the membrane center regardless of the length of membrane segment. C) Horizontal profile of the horizontal displacement of the top heads–solution surface, top heads–tails surface, tails–tails surface, bottom tails–heads surface and bottom heads–solution surface. D) Vertical profile of the horizontal displacement of the membrane in the membrane center ($x=0$ nm), and at 5 nm to the right and 5 nm to the left. The fixed charge density was -64 mC/m^2 for a 20 nm long segment and -32 mC/m^2 for a 40 nm long segment.

whereas it is under 0.003 nm when evaluated 5 nm to the right of the membrane center. This trend of the membrane being extended vertically is reversed in the upper portion of the top tails section of the bilayer, where the membrane starts to compress vertically becoming more pronounced in the top heads section of the bilayer. Thus though the membrane is extended vertically overall, it constricts in the top heads section and part of the top tails section. Qualitatively similar change is observed when the membrane segment is 40 nm long instead of 20 nm.

The horizontal deformation of the membrane though simpler is also interesting (Fig. 2C). Whereas the top membrane surface is extended the bottom membrane surface is compressed (the extension is shown as a positive horizontal displacement in the right sections of the membrane and negative in the left sections of the membrane). Moreover, as the cross-sectional plots of the horizontal displacement in the membrane center ($x=0$ nm), 5 nm to the right of the membrane center and 5 nm to the left (Fig. 2D) show the horizontal displacement (extension or compression) increases approximately linearly, as one moves from the membrane center ($z=0$ nm) upwards or downwards, though a slightly greater slope is discernible in heads sections. Membrane deformation was quantified further.

3.2. Horizontal normal strain and stress

The elastic properties of the heads and tails sections are not the same [2]. The evaluation of how these differences, which are taken into account in our simulations (see Methods), influence the normal and shear strains and stresses provide interesting insights into membrane deformation and forces determining it. Fig. 3A and D depicts 2D color coded plots of the horizontal normal strain (defined as the relative change of the horizontal length) and horizontal normal stress of the membrane bilayer with the high (64 mC/m^2) density of fixed charges (negative) on the upper membrane surface. As expected the horizontal normal strain is the highest and positive (extensive) in the upper heads section and the highest and negative (compressive) in the lower heads section. Same conclusion can be reached from the vertical cross-sectional plots of the horizontal normal strain (Fig. 3B) and from the horizontal profiles of the mean values of the horizontal normal strain (Fig. 3C). In this and in all subsequent plots the cross-sectional plots are in the membrane center (x = 0 nm), unless otherwise specified. Note that the normal strain (horizontal) of 0.01 indicates 1% change in length horizontally. The spatial profiles of the horizontal normal stress appear to be more uneven (Fig. 3D), not surprisingly given that the elastic properties of the heads and tails sections are quite different (see Table 2). Indeed, the mean values of the horizontal normal stress (Fig. 3F) demonstrate that the normal stress (horizontal) is higher in heads sections and changes faster with distance. The horizontal normal stress changes strongly with fixed charge density. The best fitted curve to the mean horizontal normal stress in the membrane center (x = 0) is meanHNS (MPa) = −0.296 + 0.023·FCD + 0.009·FCD (top heads section), and meanHNS (MPa) = −0.129 + 0.015·FCD + 0.0006·FCD (top tails section), where meanHNS is mean horizontal normal stress in MPa and FCD is fixed charge density in mC/m^2. Finally note that the normal stress of 1 MPa in the heads sections translates into tension of 0.0007 N/m, and in the tails sections into tension of 0.0013 N/m.

3.3. Vertical normal strain and stress

The vertical normal strain is the highest and positive (extensive) in the bottom heads section, and the highest and negative (compressive) in the top heads section (Fig. 4A; 2D color coded plot for the membrane bilayer with the high (64 mC/m^2) density of fixed charges (negative) on the upper membrane surface; not to scale). The vertical cross-sectional plots of the vertical normal strain (Fig. 4B) and the

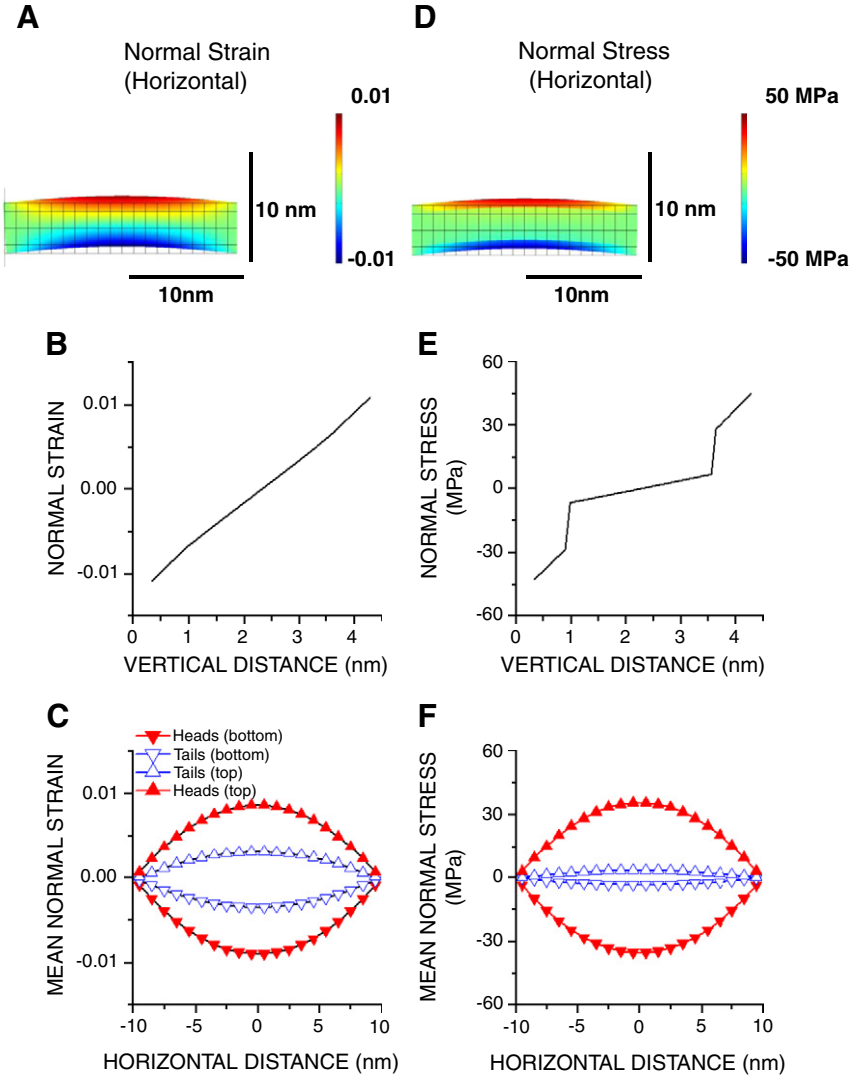

Fig. 3. 2D color plots of the horizontal normal strain (A) and stress (D) show their non-uniformity within the membrane. The horizontal normal strain is clearly extensive (positive) in the upper heads section and compressive (negative) in the lower heads sections of the membrane. B) The change of the horizontal normal strain in vertical direction is significant, but smooth. C) Horizontal profiles of the horizontal normal strain. E) The horizontal normal stress has higher values and changes more rapidly in the heads sections of the lipid bilayer. The panels in B and E show the cross-sectional vertical plots at $x = 0$ nm. The horizontal profiles of the horizontal normal strain (C), and the horizontal normal stress (F) are average values in the heads and tails sections.

horizontal profiles of their mean values (Fig. 4C) confirm this. 2D plot (Fig. 4D), the cross-sectional plot (Fig. 4E), and the horizontal profiles of the mean values (Fig. 4F) demonstrate that the vertical normal stress rises from the low (near zero) level at the bottom of the membrane to reach its peak (positive i.e. extensive) value at the top of the membrane.

3.4. Components of horizontal and vertical normal stress

The normal stress (vertical or horizontal) is determined by two contributions, one due to ε_x (ε_x is horizontal strain or gradient of *x*-displacement in *x* direction) and another due to ε_z (ε_z is vertical strain or gradient of *z*-displacement in *z* direction; [25]). Fig. 5A gives the cross-sectional vertical plots of these two contributions to the horizontal normal stress together with their sum. Fig. 5B–C shows the horizontal profiles of these contributions along the top membrane surface and bottom membrane surface, respectively. Finally, Fig. 5D depicts the cross-sectional vertical plots of these two contributions to the vertical normal stress together with their sum. Fig. 5E–F shows the horizontal profiles of the contributions to the vertical normal stress along the top membrane surface and bottom membrane surface, respectively. The horizontal normal stress is largely determined by the ε_x contribution, whereas the ε_z contribution is quite small (Fig. 5A–C). Note however that both ε_x and ε_z make the contribution to the vertical normal stress, and interestingly the contribution of the ε_x is bigger than the ε_z contribution, although the ε_z contribution is not negligible.

3.5. Shear strain and stress

Fig. 6A and D shows 2D color coded plots (not to scale) of the shear strain and stress of the membrane with high (64 mC/m^2) density of fixed charges (negative) on the upper membrane surface. Note that both the shear strain and stress appear to be higher in the tails sections than in the heads sections, and the corresponding cross-sectional vertical plots and also the horizontal plots confirm that this is indeed the case (Fig. 6B, C, E, and F). The shear strain and stress distribution within the bilayer differ if the thickness of either heads or tails sections changes. Both thicker headgroups and tails sections were tried (in one simulation the thickness of the headgroup sections increased from 0.7 nm to 1 nm, and in another the thickness of the tails sections rose from 1.3 nm to 2.0 nm). Nevertheless the distribution of the shear strain (Fig. 6B) and shear stress (Fig. 6E) remained qualitatively the same (i.e. regardless of the

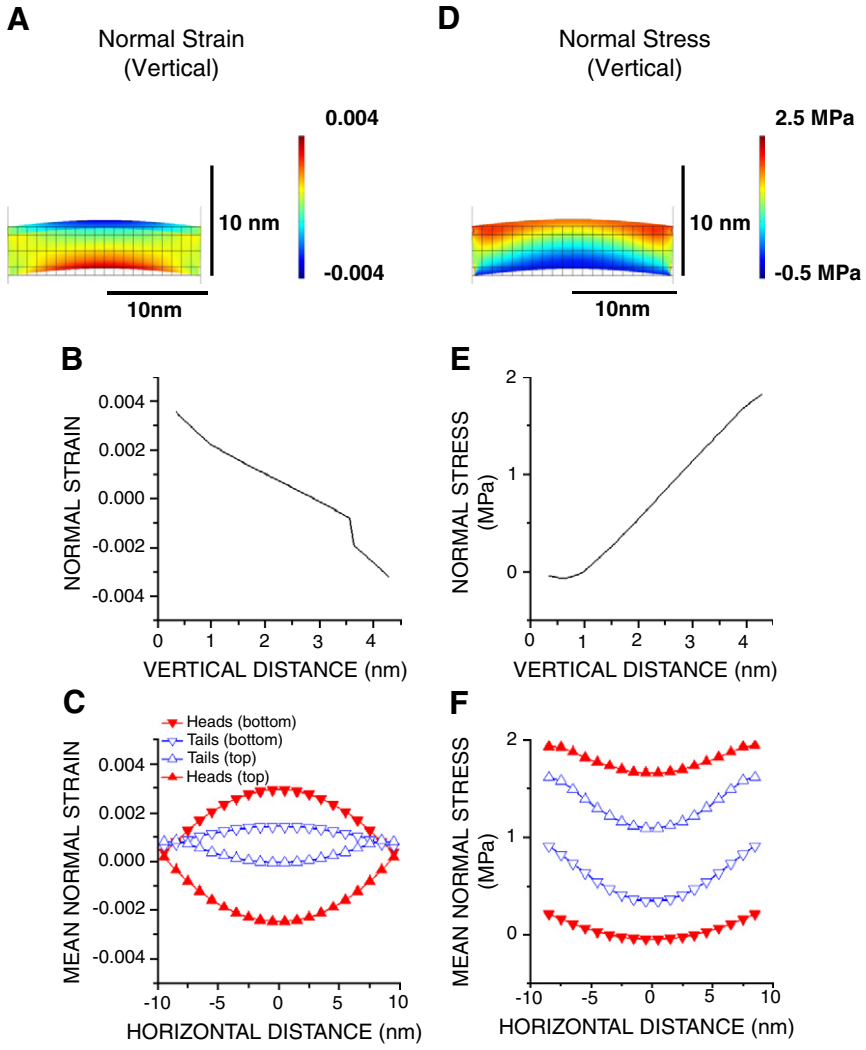

Fig. 4. 2D color plots of the vertical normal strain (A) and stress (D) reveal their non-uniformity within the membrane. The vertical normal strain is clearly compressive (negative) in the upper heads section and extensive (positive) in the lower heads sections of the membrane. B) Progressive decrease of the vertical normal strain going upwards is significant, but not entirely smooth. C) The horizontal profiles of vertical normal strain. E) The vertical normal stress increases going upwards. The panels in B and E show the cross-sectional vertical plots at $x = 0$ nm. F) The horizontal profiles of vertical normal stress. The horizontal profiles of vertical normal strain (C), and vertical normal stress (F) are average values in the heads and tails sections.

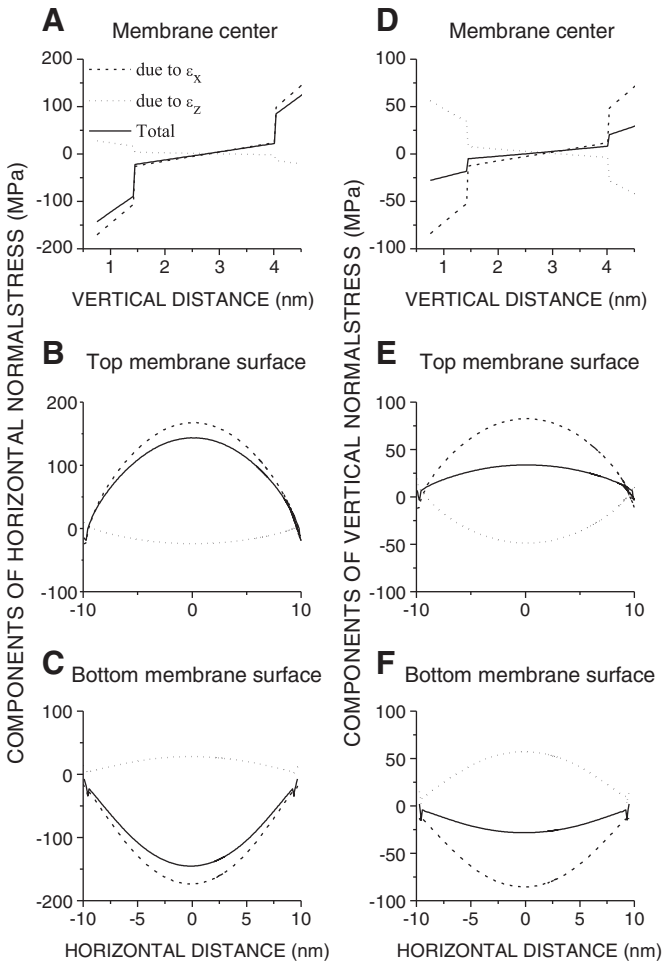

Fig. 5. The horizontal and vertical normal stress and its components. The cross-sectional vertical plots at the membrane center (at $x = 0$ nm) of the horizontal normal stress and its components (one due to ε_x and another due to ε_z; A), and of the vertical normal stress (D). The horizontal profiles of the horizontal normal stress and its components along the top membrane solution surface (B), and the bottom membrane solution surface (C). The horizontal profiles of the vertical normal stress and its components along the top membrane solution surface (E), and the bottom membrane solution surface (F).

thickness of heads or tails sections the shear strain and stress remain higher in the tails sections than in the heads sections).

3.6. Components of shear stress

Fig. 7A_1 illustrates the cross-sectional vertical plots of the two contributions to the shear stress, one due to $\delta w/\delta x$ (i.e. due to the change of vertical displacement in horizontal direction) and another due to $\delta u/\delta z$ (i.e. due to the change of horizontal displacement in vertical direction). Their sum is shown in Fig. 7A_2. Both components, as expected, have greater values in the heads sections owing to the fact that the Young modulus is greater in the heads sections. Their sum is nevertheless higher in tails sections due to the fact that their values (which are opposite in sign) are more similar in the heads sections. Same argument applies to the components of the shear stress 5 nm to the right of the membrane center, except that all values are much greater (Fig. 7C_1–C_2). Fig. 7B and D shows the horizontal profiles of the contributions to the shear stress along the top membrane surface (Fig. 7B_1), and middle membrane surface (Fig. 7D_1) with corresponding sums (Fig. 7B_2 and D_2 respectively). Two contributions, which are quite large (especially those along the top membrane surface), are opposite in sign and change in opposite direction (Fig. 7B_1 and D_1). Their sums are quite small, but significantly bigger on the surface in the middle of the membrane (tails sections).

3.7. Traction

Further understanding of the forces acting on the membrane bilayer can be gained by evaluating the spatial profiles of traction on 'virtual' horizontal and vertical edges. These are not physical partitions and exist simply for the purposes of analysis. They are not part of simulations, but only of post-processing. Fig. 8A depicts the spatial profiles of the vertical traction on horizontal edges (averaged over 1 nm horizontal sections obtained by partitioning of the heads-tails or heads-solution interfaces). The vertical traction is (as expected) the highest at the membrane top surface, where it is also quite uniform. It diminishes as one goes towards the bottom of the membrane, and at the bottom of the membrane it is almost zero. Note that the vertical traction becomes also more non-uniform at the horizontal edges in the middle of the membrane. Fig. 8B represents the spatial distribution of the horizontal traction on horizontal edges. The traction, which is clearly greater on the edges in the membrane interior, changes linearly with distance. The vertical traction on the vertical edges, which was averaged over 0.7 nm (heads sections) and 1.3 nm (tails sections), is also generally greater for the edges in the membrane interior, where it also changes more with distance (Fig. 8C). Finally, the horizontal traction on the vertical edges, which is by far the greatest, is the largest in the middle of the membrane ($x = 0$ nm), being positive for the bottom monolayer and negative for the top monolayer (Fig. 8D). The horizontal tractions and horizontal forces dominate and critically influence membrane deformation.

3.8. Elastic energy

It is clear from the 2D plot of the elastic energy density that it is not spatially uniform, but that in the heads sections it peaks in the middle of the membrane (i.e. at $x = 0$ nm; Fig. 9A). Whereas this is not surprising given that the deformation is the greatest there, it is worthwhile dissecting its contributing components. In the heads sections (both top and bottom) the elastic energy density is completely dominated by its normal horizontal component, which indeed peaks in the middle of the membrane (i.e., at $x = 0$ nm), and is essentially the same in the top and bottom sections (Fig. 9B–C). In contrast, in the tails sections its shear component is clearly the most important, although the normal horizontal component is not negligible, especially in the middle of the membrane. The shear component of the elastic energy density is however zero in the middle of the membrane in the tails sections (i.e., at $x = 0$ nm). The total elastic energy density has a minimum in the middle of the membrane, but it is not zero due to the contribution of the normal horizontal contribution. Finally, note that, and as 2D plot suggests, the elastic energy density clearly peaks in the middle of the membrane in the heads sections (top and bottom; Fig. 9F), as does the total elastic energy, which includes the contributions of the heads and tails sections (Fig. 9G).

4. Discussion

4.1. Forces acting on the charged lipid bilayer in liquid electrolyte

The main goal of these simulations is to evaluate how the elastic stresses are spatially distributed within the membrane as a result of its bending induced by the spatially uniform surface electrostatic (Coulomb and dielectric) forces [25]. The membrane, which was placed in a liquid electrolyte, was elastically complex. It was anisotropic overall, but the heads and tails sections though having different moduli, were individually both homogeneous and isotropic. These simulations thus differ from recent simulations where full anisotropy was considered [2], but the difference is negligible and the

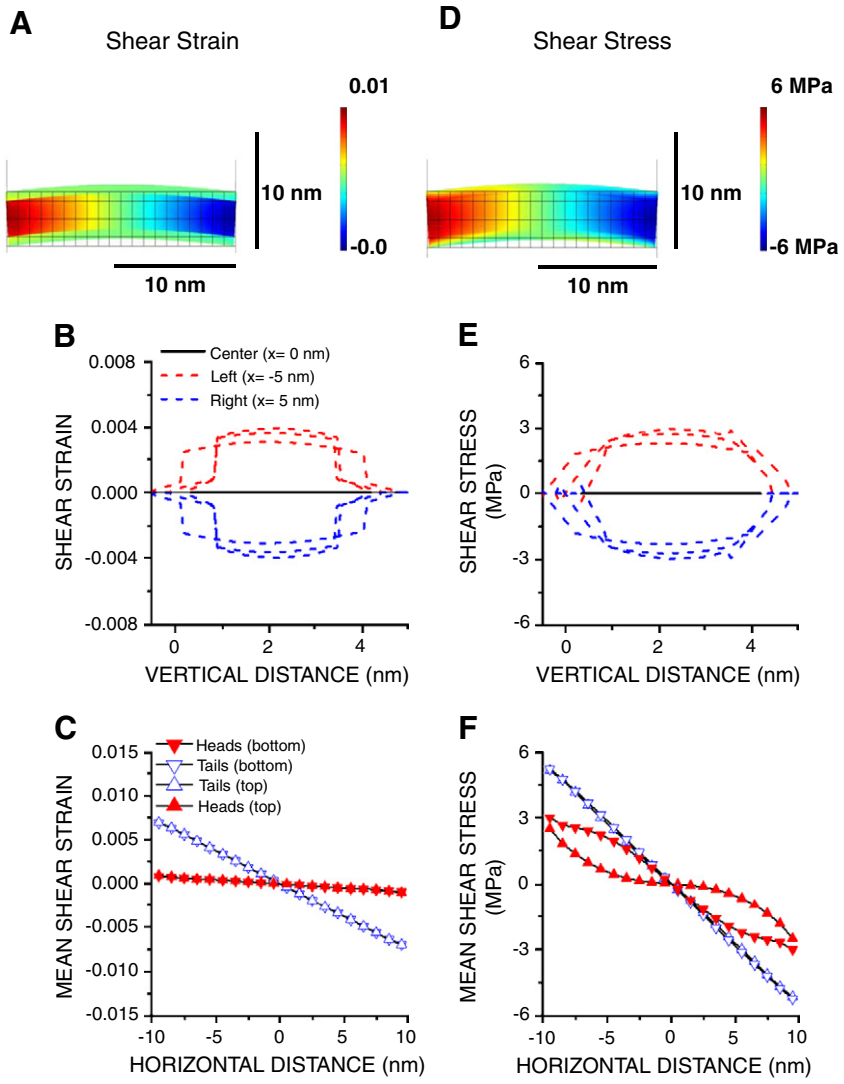

Fig. 6. The shear strain (A) and the shear stress (D) are greater in the tails sections of the lipid bilayer. B and E) Cross-sectional vertical plots in the membrane center (at $x=0$ nm), 5 nm to the right ($x=5$ nm) and to the left ($x=-5$ nm) of the shear strain (B) and shear stress (E). Note low values of shear strain and shear stress in the middle of the membrane, high and positive values in the left part of the membrane, and similarly high but negative values in the right part of the membrane. Qualitatively similar profiles are seen if either heads sections or tails sections are wider (see text). C and F) Horizontal profiles of the shear strain and the shear stress. Note that both shear strain and stress are greater in the tails sections than in the heads sections, both increase in amplitude with distance from the membrane center ($x=0$ nm), and both are positive in the left and negative in the right part of the membrane.

deformations were identical [33]. This choice however rendered the simulations faster. The electrokinetics was evaluated in the solution and the electrostatics in the whole domain (i.e. in the membrane as well as in the solution on both sides of the membrane) using a coupled system of electrostatic–electrokinetic (Poisson–Nernst–Planck) equations, and the electrostatic variables (potential, electric field, Maxwell stress tensor, Coulomb force, dielectric force and space charge density), as well as electrokinetic variables (ion concentrations) were calculated [26,27,25]. Membrane deformation is driven by: a) the Coulomb force (due to the presence of the fixed charges on the upper membrane surface and the electric field at the same surface), and b) the dielectric force (calculated from the Maxwell stress tensor at the same surface). The dielectric force, which is significantly smaller than the Coulomb force, is not negligible, and results from the uneven electric field and the membrane–water permittivity mismatch [27,25]. It always acts from the solution towards the membrane owing to much higher permittivity of water than membrane (permittivity is 80 and 2 respectively). The dielectric force at the upper membrane surface thus curtails the Coulomb force, whose direction is from the membrane towards the surface with the fixed charges regardless of the polarity of charges [25]. There is also a dielectric force at the lower surface, but it is negligible. Finally, the elastic equations were used to compute the membrane deformation, the normal (horizontal and vertical) and shear stresses and strains as well as elastic energy density.

4.2. Vertical and horizontal normal strains and stresses

Even though the external electrostatic force is spatially uniform, an evaluation of the vertical displacement reveals complexities of membrane deformation. Combined effect of the electrostatic forces (Coulomb and dielectric) is to bend the membrane upwards (i.e. towards the membrane surface with fixed charges; [25]), but all membrane sections are not equally vertically deformed. The vertical normal strain (indicating the relative change of vertical length of the unitary volume) diminishes going upwards, becoming negative in the top monolayer, and is especially low (negative) in the top heads section. The bottom monolayer is thus vertically extended, whereas the top monolayer is vertically

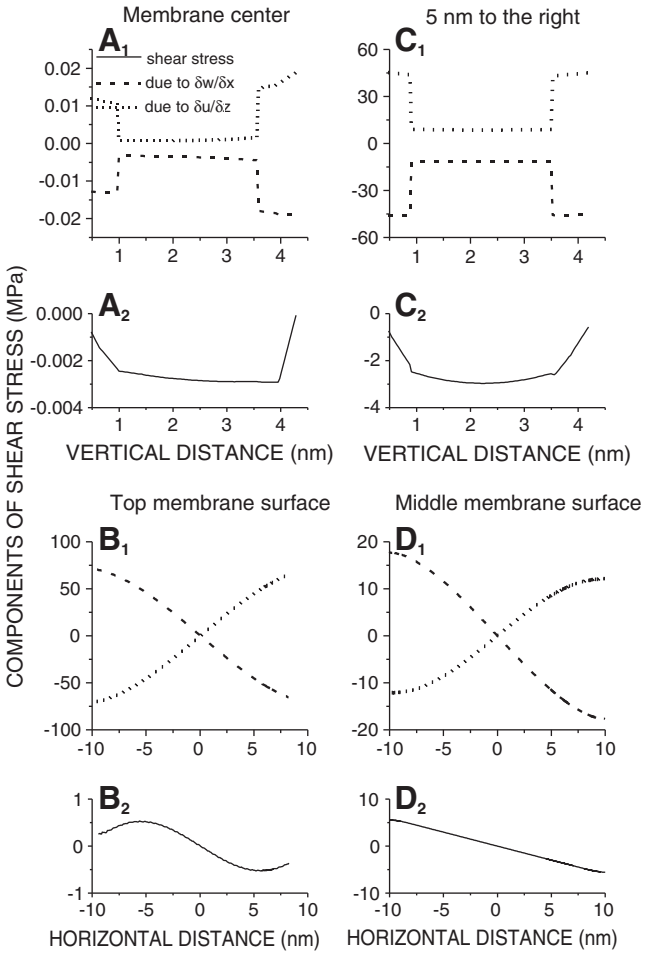

Fig. 7. The shear stress and its components. A and C) The cross-sectional vertical plots (at $x=0$ nm; A_1, and at $x=5$ nm to the right; C_1) of the contributions to the shear stress due to δw/δx (change of the vertical displacement in horizontal direction) and δu/δz (change of the horizontal displacement in vertical direction). The corresponding sums are shown below (A_2 and C_2). B and D) The horizontal profiles of the contributions to the shear stress along the top membrane solution surface (B), and along the middle membrane surface (D). Note that the contributions to the shear stress due to δw/δx and δu/δz change in opposite direction with the horizontal distance (B_1 and D_1). Their sum (i.e. the shear stress) is in both cases much smaller than individual contributions, but is still much higher along the middle membrane surface (i.e., in the tails section) than along top membrane surface (i.e. in the heads section).

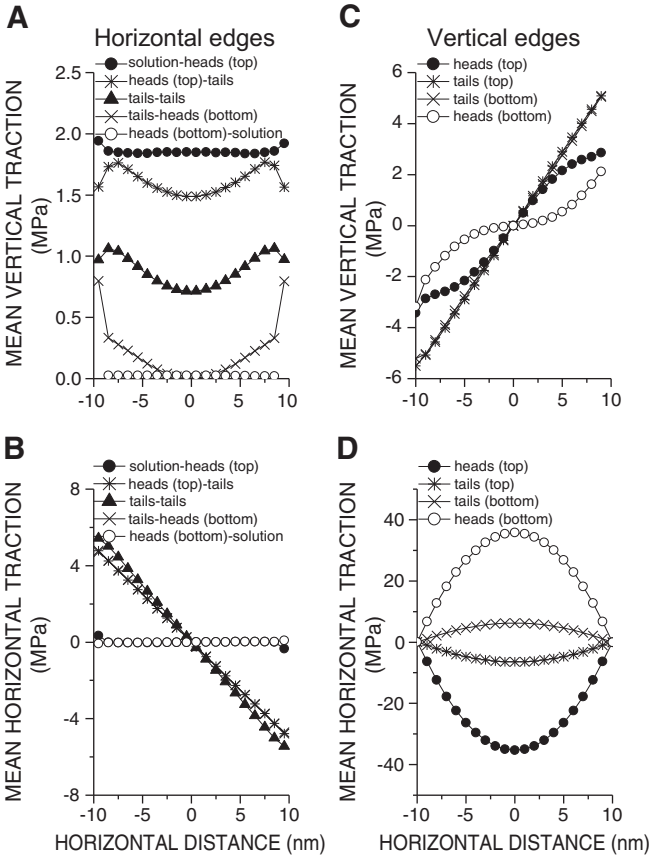

Fig. 8. The spatial distribution of traction. A) Mean vertical traction on the horizontal edges is uniform horizontally at the heads (top) – solution surface, but is non-uniform in the interior of the membrane. On all horizontal surfaces it presses downwards. B) Mean horizontal traction on the horizontal edges is much greater on the edges in the membrane interior, than on the edges on the membrane surface. Note that it is positive in the left section of the membrane and negative in the right section on all interior horizontal edges. C) Mean vertical traction is also greater on the vertical edges of the membrane interior (the tails sections), but the traction on the external edges (the heads sections), though smaller is not negligible. In both cases the traction acts downwards (i.e. it is positive in the part of the membrane on the right and negative in the part on the left). D) Mean horizontal traction, which is by far the greatest, is negative on the vertical edges of the top monolayer (both heads and tails sections) and positive on the vertical edges of the bottom monolayer (both the heads and tails sections). The peak value is in all cases in the center of the membrane ($x=0$ nm).

compressed, and this pattern of extension–compression does not depend on how long the membrane section is used for simulations. Its horizontal change is different, and has near zero values at both ends (left and right) and either a minimum (top monolayer) or a maximum (bottom monolayer) in the middle of the membrane (i.e. equidistantly from the left and right end). The horizontal normal strain (indicating the relative change of horizontal length of the unitary volume) increases almost linearly going upwards. Its horizontal profile is different, zero at both ends and with either a minimum (bottom monolayer) or a maximum (top monolayer) in the middle of the membrane. The membrane thus extends horizontally and compresses vertically in the top monolayer, whereas opposite is the case in the bottom monolayer.

The evaluation of stress profiles and a comparison of the stress and strain profiles provide additional insights. Stress is a tensor property, and on every surface in a bilayer it can be split up in one component normal to the plane (normal stress), and two (perpendicular) components in the plane (shear stress; [29]). Moreover, the normal strain and normal stress of any plane are related (directly), but the normal strains of planes perpendicular to the plane studied also contribute (indirectly) to the normal stress. The indirect contributions depend on the Poisson ratio, which defines how much a material that is extended (or compressed) in one direction, will compress (or extend) in other two directions. The ratio is taken to be 0.33 for a bilayer (see Table 2). These contributions were compared. Given that the vertical normal strain is much smaller than horizontal normal strain, the vertical normal stress is likely to be smaller than horizontal normal stress, and it is. Nevertheless, the vertical normal stress and the vertical normal strain profiles are not similar owing to the contribution of the horizontal normal strain, which influences (indirectly) the vertical normal stress more than the vertical normal strain does (directly). The horizontal normal stress is however largely associated with the horizontal normal strain, which is as a rule greater than vertical normal strain.

4.3. Shear stress

The shear stress is an index of where the membrane is most likely to deform by sliding along a plane parallel to the imposed stress [29,26]. Its evaluation is of interest because high shear stress may suggest where the embedded proteins or lipids will 'experience' such an influence and be modified by the membrane. The most surprising finding of this study is that the shear stress is greater in the tails than in the heads sections. We expected the opposite because the Young modulus is greater

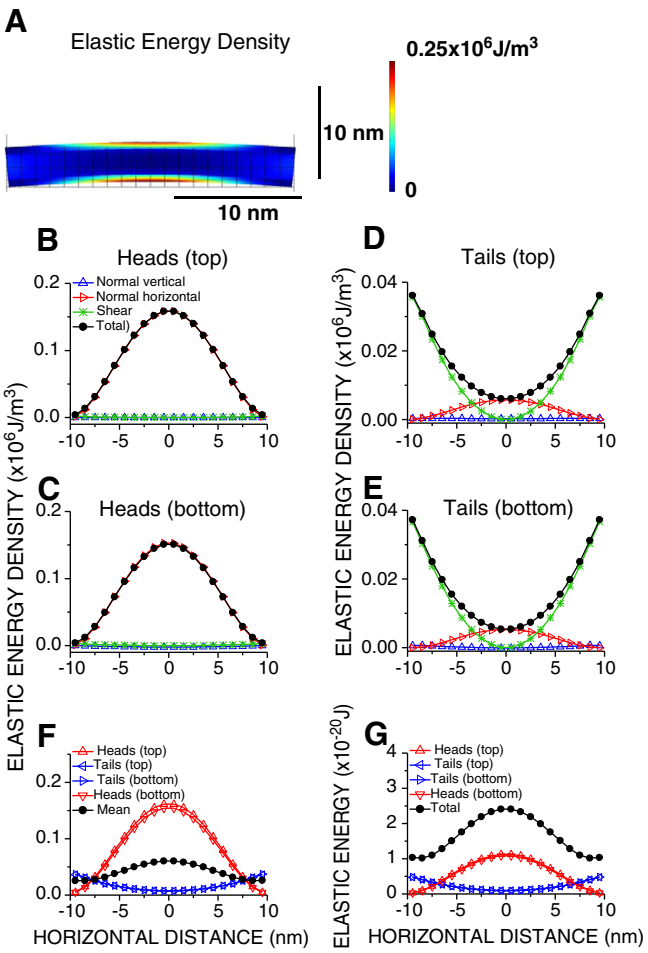

Fig. 9. Spatial distribution of the elastic energy density and the elastic energy. A) 2D plots of the elastic energy density. B–C) The total elastic energy density and its normal horizontal, normal vertical and shear components in the heads section of the top (B) and bottom (C) monolayer. D–E) The total elastic energy density and its normal horizontal, normal vertical and shear contributions in the tails section of the top (D) and bottom (E) monolayer. Note that in the heads sections the elastic energy density is completely dominated by the horizontal normal contribution. In contrast in the tails sections the shear component is clearly the most important, but the horizontal normal contribution is not negligible, especially in the middle of the membrane. F) The elastic energy density in the heads and tails sections and the mean elastic energy density for the whole membrane. G) The elastic energy in the heads and tails sections and the total elastic energy of the whole membrane.

in the heads section, and the shear stress is proportional to the Young modulus [25]. Note also that we also evaluated whether this remains valid if the thickness of the tails sections increased from 1.3 nm to 2.0 nm, and also if the thickness of the heads sections increased from 0.7 nm to 1.0 nm, and it did. Two factors contribute to the shear stress: a) change of vertical displacement in horizontal direction, and b) change of horizontal displacement in vertical direction. Their comparison provides the explanation. Although both are individually smaller in the tails sections, their values differ more from each other, and being opposite in sign add to a greater total value.

4.4. Traction

Spatial profiles of the normal and shear stress reveal how the forces that compress/extend and deform the membrane are distributed within the bilayer. Nevertheless, we also evaluated what the forces (vertical and horizontal) are on the 'virtual' vertical or horizontal edges (i.e. on the edges that are not physical) within the membrane bilayer, as such estimates may be intuitively more understandable. Briefly, the spatial profiles of the vertical traction on the horizontal edges are similar to those of the vertical normal stress, but are not identical owing to averaging (which is different in two cases — one is on the surfaces sections and another on the volume sections), and more importantly because the vertical traction on the horizontal edges is determined not only by the vertical normal stress, but also by the shear stress. Similar reasoning applies when comparing the horizontal traction on the vertical edges with the horizontal normal stress, but in the later case the difference is negligible, because the shear stress contribution is relatively much smaller.

4.5. Elastic energy profiles and their components

The elastic energy of the membrane is the potential energy stored in the shape of the membrane. It reflects the work needed to achieve such a shape, but also the work that can be done when the membrane returns to its 'original' shape. On the molecular level it reflects the storage of energy caused by the change of the inter-atomic distances between nuclei. It is useful as an overall measure of where the membrane is extended/compressed and deformed, and it has been used to evaluate membrane bilayer–protein interactions. However, correlation of the membrane elastic energy with function of proteins embedded in the membrane gave mixed results. The function of rhodopsin reconstituted into bilayer could be explained by the changes of the elastic energy of the membrane, but only partially [36], but the function of the secondary multidrug transporter LmrP of *Lactococcus lactis* appears not to depend on the elastic energy of the membrane, but on the hydrogen bonding of interfacial headgroups [37]. Moreover, the activation of the large conductance mechanosensitive channel of *Escherichia coli* does not scale with membrane spontaneous curvature, but with the ability of the annular lipid headgroups to form hydrogen bonds with the channel [38]. Given that the elastic energy has three components (normal vertical, normal horizontal and shear [29,25]), which have very different values and spatial profiles, and that the elastic energy does not distinguish extension from compression, or these two from deformation, the interpretation of elastic energy vs. protein function relationship is not simple. Moreover the extension in one monolayer is associated with compression in another monolayer.

In both (top and bottom) heads sections the total elastic energy density distributions, which are dominated by the horizontal normal component, peak in the middle of the membrane, and are zero at both ends. This is as expected because the elastic energy density is a product of the horizontal normal stress and strain, and both have such profiles. The elastic energy density is smaller in the tails sections, its profiles are different, higher at both ends, but lower though not zero in the middle of the membrane. This is also as expected, as the elastic energy is dominated by the shear stress and strain components, and their profiles are similar to those of the elastic energy density. The elastic energy density is not zero in the membrane center, and this is due to the contribution of the horizontal normal elastic energy. Finally, the normal vertical component of the elastic energy density is very small in both the heads and in the tails sections, as are the values of the vertical normal stress and strain that determine it.

5. Conclusion

Even spatially uniform and constant external force leads to a complex deformation and generates complex spatial profiles of stresses (shear and normal), traction and of the elastic energy, when the difference of elastic properties of the heads and tails sections of the membrane bilayer are taken into account. Distinguishing where the normal stresses (horizontal or vertical) are the greatest, whether they are compressive or extensive, but also where the shear stresses are prominent can be very important in predicting where and how the membrane interacts with the embedded proteins and lipids, which more commonly used elastic energy does not discriminate adequately. This is of special relevance since there is a large and growing

body of evidence demonstrating such interactions, whereas our understanding of such processes is still rudimentary. In future studies we will further characterize such interactions, but with the proteins embedded in the membrane.

Acknowledgements

This work was supported by the grant from the National Sciences and Engineering Research Council of Canada and Canadian Heart and Stroke Foundation to M.I.G.

References

[1] W. Helfrich, Elastic properties of lipid bilayers—theory and possible experiments, Z. Naturforsch. C 28 (1973) 693–703.
[2] F. Campello, H.T. McMahon, M.M. Kozlov, The hydrophobic insertion mechanism of membrane curvature generation by proteins, Biophys. J. 95 (2008) 2325–2339.
[3] T. Kirchhausen, Three ways to make a vesicle, Nat. Rev. Mol. Cell Biol. 1 (2000) 187–198.
[4] J. Zimmerberg, M.M. Kozlov, How proteins produce cellular membrane curvature, Nat. Rev. Mol. Cell Biol. 7 (2006) 9–19.
[5] T. Ursell, K.C. Huang, E. Peterson, R. Phillips, Cooperative gating and spatial organization of membrane proteins through elastic interactions, PLoS Comput. Biol. 3 (2007) 803–812.
[6] D. Marsh, Lateral pressure profile, spontaneous curvature frustration, and the incorporation and conformation of proteins in membranes, Biophys. J. 93 (2007) 3884–3899.
[7] O.S. Andersen, R.E. Koeppe II, Bilayer thickness and membrane protein function: an energetic perspective, Annu. Rev. Biophys. Biomol. Struct. 36 (2007) 107–130.
[8] M.O. Jensen, O.G. Mouritsen, Lipids do influence protein function — the hydrophobic matching hypothesis revisited, Biochim. Biophys. Acta 1666 (2004) 205–226.
[9] E. Perozo, A. Kloda, D.M. Cortes, B. Martinac, Physical principles underlying the transduction of bilayer deformation forces during mechanosensitive channel gating, Nat. Struct. Biol. 9 (2002) 696–703.
[10] K. Yoshimura, T. Nomura, M. Sokabe, Loss-of-function mutations at the rim of the funnel of mechanosensitive channel MscL, Biophys. J. 86 (2004) 2113–2120.
[11] T. Nomura, M. Sokabe, K. Yoshimura, Lipid–protein interaction of the MscS mechanosensitive channel examined by scanning mutagenesis, Biophys. J. 91 (2006) 2874–2881.
[12] V. Vásquez, M. Sotomayor, J. Cordero-Morales, K. Schulten, E. Perozo, Structural mechanism for MscS gating in lipid bilayers, Science 321 (2008) 1210–1214.
[13] F. Maingret, A.J. Patel, F. Lesage, M. Lazdunski, E. Honore, Lysophospholipids open the two-pore domain mechano-gated K1 channels TREK-1 and TRAAK, J. Biol. Chem. 275 (2000) 10128–10133.
[14] K. Hayakawa, H. Tatsumi, M. Sokabe, Actin stress fibers transmit and focus force to activate mechanosensitive channels, J. Cell Sci. 121 (2008) 496–503.
[15] S.M. Bezrukov, R.P. Rand, I. Vodyanoyc, V.A. Parsegian, Lipid packing stress and polypeptide aggregation: alamethicin channel probed by proton titration of lipid charge, Faraday Discuss. 111 (1998) 173–183.
[16] S. Taheri-Araghi, B.Y. Ha, Electrostatic bending of lipid membranes: how are lipid and electrostatic properties interrelated? Langmuir 26 (2010) 14737–14746.
[17] M. Goulian, O.N. Mesquita, D.K. Fygenson, C. Nielsen, O.S. Andersen, A. Libchaber, Gramicidin channel kinetics under tension, Biophys. J. 74 (1998) 328–337.
[18] C. Chen, R. Xu, I.J. Clarke, M. Ruan, K. Loneragan, S.G. Roh, Diverse intracellular signalling systems used by growth hormone-releasing hormone in regulating voltage-gated Ca2+ or K channels in pituitary somatotropes, Immunol. Cell Biol. 78 (2000) 356–368.
[19] R. Kwiecien, C. Hammond, Differential management of Ca^{+} oscillations by anterior pituitary cells: a comparative overview, Neuroendocrinology 68 (1998) 135–151.
[20] S. Ben-Tabou De-Leon, E. Blotnick, I. Nussinovitch, Effects of osmotic swelling on voltage-gated calcium channel currents in rat anterior pituitary cells, Am. J. Physiol. Cell Physiol. 285 (2003) C840–C852.
[21] J. Dai, H.P. Ting-Beall, M.P. Sheetz, The secretion-coupled endocytosis correlates with membrane tension changes in RBL 2H3 cells, J. Gen. Physiol. 110 (1997) 1–10.
[22] G. Kilic, Exocytosis in bovine chromaffin cells: studies with patch-clamp capacitance and FM1-43 fluorescence, Biophys. J. 83 (2002) 849–857.
[23] D. Schmidt, R. MacKinnon, Voltage-dependent K channel gating and voltage sensor toxin sensitivity depend on the mechanical state of the lipid membrane, Proc. Natl. Acad. Sci. 105 (2008) 19276–19281.
[24] G. Apodaca, Modulation of membrane traffic by mechanical stimuli, Am. J. Physiol. Ren. Physiol. 282 (2002) F179–F190.
[25] M. Tajparast, M.I. Glavinović, Elastic, electrostatic and electrokinetic forces influencing membrane curvature. Biochim Biophys Acta (2011) (Submitted for publication).
[26] G. Karniadakis, A. Beskok, N. Aluru, Microflows and nanoflows, Fundamentals and Simulation, Springer, 2005.
[27] K.H. Kang, D. Li, Dielectric force and relative motion between two spherical particles in electrophoresis, Langmuir 22 (2006) 1602–1608.
[28] M. Tajparast, M.I. Glavinović, Extrusion of transmitter, water and ions generates forces to close fusion pore, Biophys. Biochem. Acta 1788 (2009) 993–1008.
[29] A.I. Lurie, Theory of Elasticity, Springer Verlag, 1999.
[30] M. Wissler, E. Mazza, Mechanical behavior of an acrylic elastomer used in dielectric elastomer actuators, Sensors and Actuators A 134 (2007) 494–504.
[31] G. Kofod, The static actuation of dielectric elastomer actuators: how does pre-stretch improve actuation? J. Phys. D Appl. Phys. 41 (2008) 1–11.
[32] T. Chou, M.V. Jaric, E.D. Siggia, Electrostatics of lipid bilayer bending, Biophys. J. 72 (1997) 2042–2055.
[33] M. Tajparast, M.I. Glavinović, Forces and stresses acting on fusion pore membrane during secretion, Biophys. Biochem. Acta 1788 (2009) 1009–1023.
[34] S.G.A. McLaughlin, G. Szabo, G. Eisenman, Divalent ions and the surface potential of charged phospholipid membranes, J. Gen. Physiol. 58 (1971) 667–687.
[35] B. Hille, A.M. Woodhull, B.I. Shapiro, Negative surface charge near sodium channels of nerve: divalent ions, monovalent ions, and pH, Philos. Trans. R. Soc. Lond. B Biol. Sci. 270 (1975) 301–318.
[36] O. Soubias, W.E. Teague, K.G. Hines, D.C. Mitchell, K. Gawrisch, Contribution of membrane elastic energy to rhodopsin function, Biophys. J. 99 (2010) 817–824.
[37] P. Hakizimana, M. Masureel, C. Govaerts, Interactions between phosphatidylethanolamine headgroup and LmrP, a multidrug transporter: a conserved mechanism for proton gradient sensing? J. Biol. Chem. 283 (2008) 9369–9376.
[38] A.M. Powl, J.M. East, A.G. Lee, Importance of direct interactions with lipids for the function of the mechanosensitive channel MscL, Biochemistry 47 (2008) 12175–12184.